

# Different behaviors of wavelet results for type-B and type-C QPOs of MAXI J1535-571 based on NICER data

X. Chen<sup>a</sup>, W. Wang<sup>a,b</sup>

<sup>a</sup>Department of Astronomy, School of Physics and Technology, Wuhan University, Wuhan, 430072, China

<sup>b</sup>E-mail: wangwei2017@whu.edu.cn

## Abstract

Wavelet analysis, in addition to power density spectra, is another method to study the quasi-periodic signals in the light curves, but has been rarely used in black hole X-ray transients. We performed wavelet analysis of X-ray timing features and quasi-periodic oscillations (QPOs) based on NICER observations of the black hole candidate MAXI J1535-571 in this paper. Separating the light curves by the confidence level of wavelet results, we find significant differences exist in the PDS, hardness ratio and mean count between light curve segments above and below the confidence level. The S-factor, which is defined as the ratio of the effective oscillation time and the total time, demonstrates distinct values between type-C and type-B QPOs. Based on our results, the S-factor for type-B QPO is very close or equal to 0, no matter the confidence level is set as 95% or 68%, while the S-factor of type-C QPO is significantly higher, especially in the 68% confidence level case. We discuss the implications of the wavelet results on resolving type-B and type-C QPOs in black hole X-ray binaries.

**Keywords:** Black holes physics, X-rays: binaries, Stars: MAXI J1535-571

## 1. Introduction

Stellar-mass black holes (BHs) in X-ray binaries normally spend most of their time in a quiescent state with a low luminosity, and can only be detected during their short lasted outbursts, which usually have their flux increased by several orders of magnitude (Remillard and McClintock, 2006) in a few months, hence only around 70 stellar mass BHs are reported so far (Corral-Santana et al., 2016). A typical outburst goes through several states, showing different properties in light curves and spectra (Homan and Belloni, 2005), including the low-hard state (LHS), hard-intermediate state (HIMS), soft-intermediate state (SIMS) and high-soft state (HSS) (Belloni et al., 2011), and normally forms a "q"-shape in the hardness intensity diagram (Fender et al., 2004).

Quasi-periodic Oscillations (QPOs; van der Klis, 1989; Nowak, 2000; Ingram and Motta, 2019)) sometimes appear in the X-ray light curves during the outburst and are generally studied with the power density spectrum (PDS) in the Fourier domain. These QPOs are classified as low-frequency QPOs (LFQPOs) with central frequencies less than 30 Hz, and high-frequency QPOs (HFQPOs) with central frequencies normally greater than 60 Hz, but are less common compared to LFQPOs (Belloni and Stella, 2014). The more frequently studied LFQPOs are divided into three classes depend on their properties such as the rms, the quality factor, the centroid frequency and so on, called type-A, -B and -C (Wijnands et al., 1999; Casella et al., 2004, 2005; Remillard et al., 2002). Type-C QPOs can appear in all states, but are mostly in the LHS and HIMS (Motta, 2016), with high rms (up to 20%) and wide range of centroid frequency (0.01-30 Hz). Type-B QPOs has lower

rms (less than 5%) with centroid frequency around 6 Hz. Their PDS contains weak red noise. Basically, they only appear in the SIMS, and are the characteristic that distinguishes the SIMS from HIMS (Belloni and Motta, 2016). Type-A QPOs are even weaker and quite rare, and are commonly noticed in the HSS.

PDS has been widely used on QPO study for decades, and provides plenty of instructive results. However, the physical origin of QPOs is still under debate, such as the instabilities in the disk (Tagger and Pellat, 1999), oscillations in the corona (Cabanac et al., 2010), the Lense-Thirring precession of the hot inner flow (Ingram et al., 2009; Veledina et al., 2013; Ingram et al., 2016, 2017), or the coupling of the accretion disc and the Comptonizing corona (Karpouzas et al., 2020; Bellavita et al., 2022; Méndez et al., 2022; García et al., 2021; Zhang et al., 2022). In addition, different types of QPOs may originate with different mechanism. For example, type-B QPO are generally believed to be jet related (e.g. Stevens and Uttley, 2016; de Ruiter et al., 2019), and have different physical origins with type-C, while type-A and type-C QPOs may share the same generation process (Motta et al., 2011, 2012). Hence the QPO classification is of great importance in understanding their generation.

The PDS based QPO classification identifies QPO types based on the evolution of the rms, the quality factor, the centroid frequency, the existence of the red noise component etc. However, PDS normally are spiky and noisy, especially in the lower frequency part, which makes it hard to recognise the red noise and/or even the QPO peak. To solve this problem, the averaged PDS, i.e. averaging the PDS of each segmented light curve, is performed, which requires that the total time duration of the light curve cannot be short, otherwise there will not

be enough segments to be averaged. Moreover, it assumes the PDS of each averaged segment contains the same information, which means the QPO and the band-limited noise properties cannot evolve with time. Another flaw for both PDS and averaged PDS is that, the chosen segment of the light curve cannot be very short (such as 1 s or less), otherwise the result will not be trustworthy. With all the possible flaws, sometimes it is not easy to quantitatively distinguish the QPO types (e.g. the quality factor of type C QPOs, see Bogensberger et al., 2020).

Wavelet analysis is a common tool to study the variation of power in a given time series in many research fields such as geophysics, and has been used to study the QPO of XTE J1550–564 (Lachowicz and Done, 2010) and IGR J17091–3624 (Katoch et al., 2021). While Fourier transform is extremely useful and accurate in searching for periodic signals, wavelet transform can handle irregular and non-continuous signals very well, such as the fast variations of QPOs. However, many studies using wavelet or Fourier transforms have suffered from quantitatively distinguishing valid signals. Hence Torrence and Compo (1998) provided a solution for statistical significance testing that can be used in wavelet analysis. Using this method, transient QPO behaviors can be well studied (Chen et al., 2022a). In addition, Chen et al. (2022b) studied the wavelet results of QPO in the source MAXI J1535–571 during its 2017 outburst with Insight-HXMT observations. Separating time series by confidence interval calculation, they found that the QPOs appear and disappear in seconds for the whole nine observations with QPO detected, which has not been observed before. This difference are also notable in PDS shape, rms, hardness ratio and spectra. Flip-flop perhaps is the most related phenomenon, even though it normally takes several tens of seconds to transit states. However, flip-flop is poorly understood, because only several sources have showed this kind of behavior so far, and they exhibit quite different properties (Miyamoto et al., 1991; Nespoli et al., 2003; Takizawa et al., 1997; Homan et al., 2001; Sriram et al., 2016; Casella et al., 2004; Sriram et al., 2013; Homan et al., 2005; Sriram et al., 2012; Kalamkar et al., 2011; Bogensberger et al., 2020; Yang et al., 2022).

MAXI J1535–571 was discovered by MAXI/GSC (Negoro et al., 2017a) and Swift/BAT (Kennea et al., 2017) during its 2017 outburst. The following multi-band observations suggest that MAXI J1535–571 is a low-mass X-ray binary (Negoro et al., 2017b; Scaringi and ASTR211 Students, 2017; Dinçer, 2017; Russell et al., 2017) located around 4 kpc away (Chauhan et al., 2019). It contains a near-maximally spinning black hole, and is perhaps viewed at a high inclination (Miller et al., 2018; Xu et al., 2018; Dong et al., 2022). Different types of QPOs have been studied in this source (Gendreau et al., 2017; Mereminskiy et al., 2018; Stiele and Kong, 2018; Huang et al., 2018; Bhargava et al., 2019), and found a possible link between the QPO type change from type-C to type-B and the discrete jet launching (Russell et al., 2019). The main outburst ended in May 2018, followed by several re-flares which also contains a state transition (Parikh et al., 2019; Cúneo et al., 2020).

In this paper, we analyze the Neutron Star Interior Composition Explorer (NICER; Gendreau et al., 2016) observations of MAXI J1535–571 using wavelet analysis. We have improved

Observation ID	MJD start	Exposure (s)
1050360103	58005.30	502
1050360104	58008.46	5405
1050360105	58008.99	10710
1050360106	58010.00	6570
1050360107	58011.87	1787
1050360108	58012.19	3617
1050360109	58013.22	4671
1050360110	58014.05	3415
1050360111	58015.28	2159
1050360112	58016.24	2888
1050360113	58017.01	6342
1050360114	58018.37	2337
1050360115	58019.01	9808
1050360116	58020.05	6718
1050360117	58021.02	5441
1050360118	58022.24	4321
1050360119	58023.25	4098
1050360120	58020.57	4142
1130360101	58024.74	2509
1130360102	58025.76	1694
1130360103	58026.73	3667
1130360104	58027.75	1839
1130360105	58028.72	5835
1130360106	58029.75	4131
1130360107	58030.72	4440
1130360108	58031.36	3838
1130360109	58032.38	3477
1130360110	58033.03	7686
1130360111	58034.00	7283
1130360112	58035.16	4931
1130360113	58036.13	5153
1130360114	58037.03	6408
1130360115	58038.00	1385
1130360116	58065.71	141

Table 1: NICER observations of MAXI J1535–571 used in this paper.

the calculation method of QPO confidence intervals in wavelet in order to remove the influence of broad band noise (BBN). We describe this improvement in Section 2, along with the observations and data reductions. Wavelet results are shown in Section 3. In Section 4, we discuss the possible indication of the wavelet results. Finally a conclusion is made in Section 5.

## 2. Observations and Data reduction

We used all the NICER observations of MAXI J1535–571 in 2017 in this paper, and the observation IDs are listed in Table 1. The standard NICER processing pipeline `nicerl2` and `nicerl3-lc` are used to process the data, while the CALDB version is `xti20221001`. The detectors of #14 and #34 are removed as recommended.

Wavelet analysis (Torrence and Compo, 1998) is used for the 1–10 keV band light curve analysis, while the time resolution

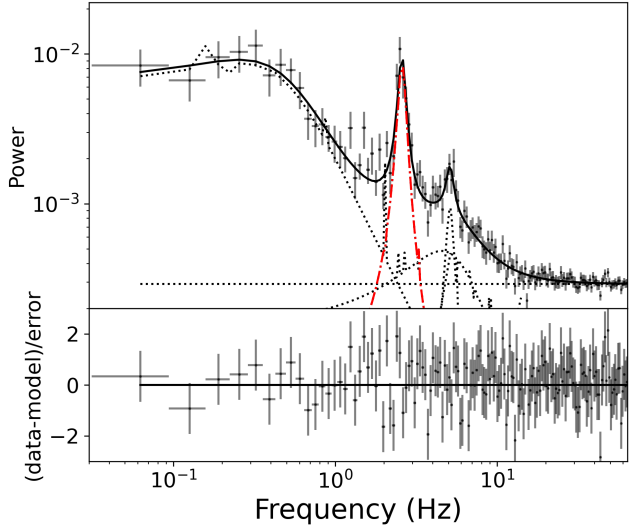


Figure 1: The 16 s averaged PDS fitting result of the first GTI in obsID 1050360104. The dashed lines show the components, while the red one marks the QPO component.

is 0.0078125 s. Each NICER observation is typically divided into a dozen to several tens of Good Time Intervals (GTIs) after the data processing, with relatively long gaps between these intervals. Wavelet analysis is not capable of handling such gaps, thus it is necessary to apply wavelet analysis separately to each interval. We set Morlet wavelet as the ‘mother’ wavelet with  $m = 6$ , and the 95 percent significance level is calculated by the univariate lag-1 autoregressive (see Chen et al., 2022b, for more technique details).

However, as can be seen from Chen et al. (2022b,a), the BBN sometimes can also be identified as valid signals. This will obviously have an impact on the QPO confidence level calculation of the wavelet results, especially for lower energy band below 10 keV, lower QPO frequency or very weak QPO signals such as the type-B QPOs in MAXI J1535-571 as reported by Stevens et al. (2018) and Zhang et al. (2023). In order to remove the influence of BBN to more accurately distinguish the time that includes QPO from the time that does not include QPO, we perform a QPO component extraction method on the wavelet results. We take the first GTI (around 220 s) in obsID 1050360104 as an example to explain our QPO component extraction method. We first calculate the averaged power density spectrum (PDS) of the GTI with 16 second time segments, with rms-squared normalization (Belloni and Hasinger, 1990) been applied. We then fit this averaged PDS with multi-Lorentzian function and a constant white noise using XSPEC v12.13.0c, see Figure 1. After picking out the QPO component (if any, which is the red line in Figure 1), we calculate the proportion curve of QPO component, and apply it on the local wavelet power of the GTI, which leaves only the QPO component in the wavelet power. Meanwhile, we leave the 95% confidence level results unchanged. We then repeat the above steps for all the other GTIs of 1050360104 and other observations.

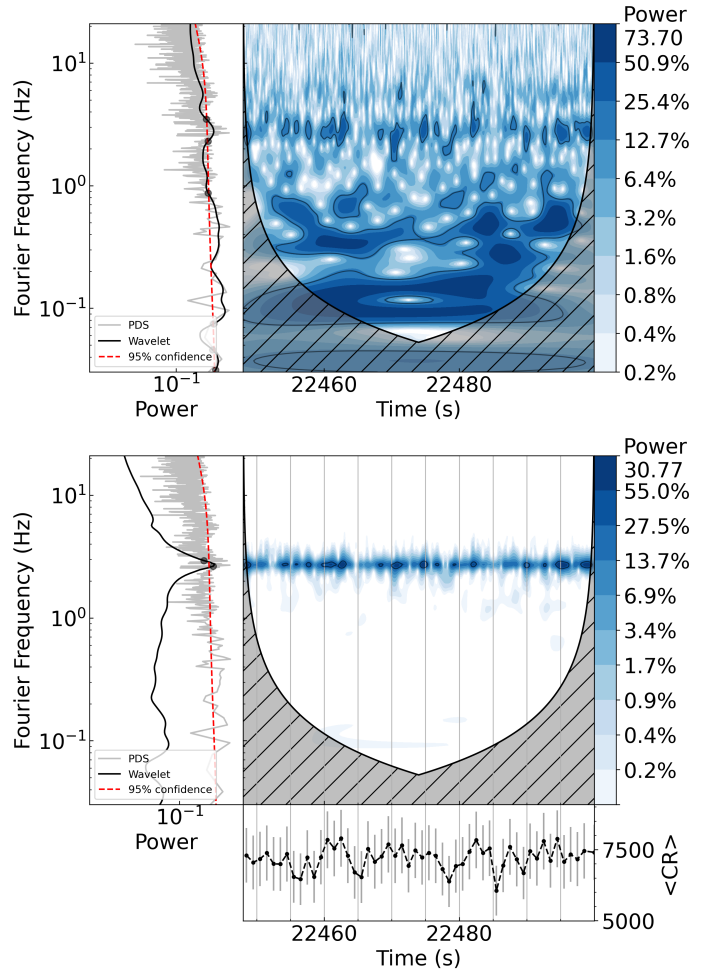


Figure 2: Wavelet results before (top panel) and after (bottom panel) QPO component extracted. The light curve is a very short GTI from observation 1050360104 in 1-10 keV. In each sub panel, PDS (grey line), global wavelet spectrum (black line), 95 percent confidence level (red line), and local wavelet spectrum (right side) are shown. In the local wavelet spectra, the black line circled area contains significant power with confidence level greater than 95 percent, and the grey hashed area represent the cone of influence. In the color bar, we show the maximum power of the local wavelet spectrum on the top, and the underneath values are the percentage of the maximum. In the bottom panel, we add the mean count rate evolution in 1-10 keV band averaged every second.

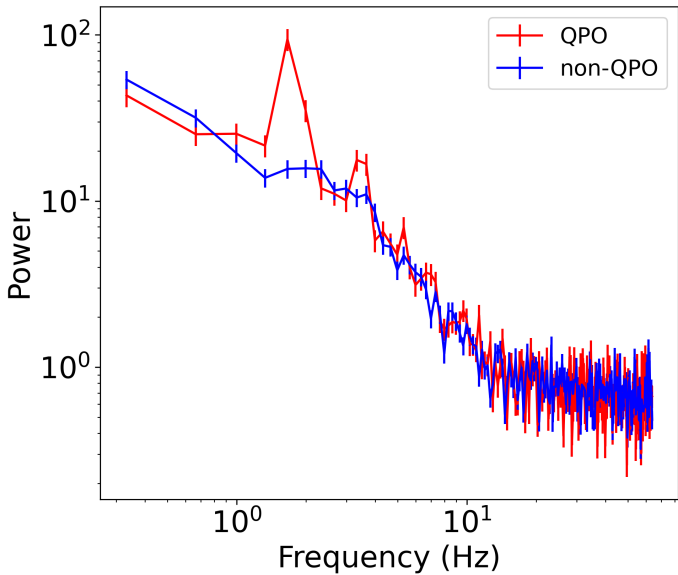


Figure 3: 3 seconds averaged PDS for the first GTI in obsID 1050360106. The PDS of QPO time and non-QPO time is separated by wavelet analysis and shown with red line and blue line, respectively. Leahy normalization is performed without white noise subtracted. The wavelet is performed with 95% confidence level.

### 3. Results

In Figure 2, we show the wavelet results before and after the QPO component extracted. It is clearly shown in the plots that after the QPO extraction process, the area exceeding the confidence level is significantly reduced, especially below 1 Hz. We present a very short interval here of around 50 s in 1050360104 to clearly exhibit the relationship between wavelet power levels and mean count rates. The circled area in the local wavelet plot, which means the power inside exceeds the 95% confidence level, matches the "peaks" in the mean count rate very well for most of the cases, indicating a possible link between the significant power and the count rate. However, if we take the large error bars in the bottom panel into consideration, the conclusion may not be certain, but it may also explain why count rate peaks sometimes do not match the significant power.

We compare time with significant power (hereafter QPO time) and time with insignificant power (hereafter non-QPO time) in each GTI. We notice the QPO time always have higher mean counts ( $\sim 3$  in 1-10 keV) and higher hardness ratio ( $\sim 0.002$  in 7-10 keV / 1-2 keV), and the distinction can be also noticed in the PDS. For most of the observations, obvious peaks can be noticed in the QPO PDS around the QPO frequency and/or its harmonics, while the peaks almost cannot be seen in the non-QPO PDS. In Figure 3, we show such an example.

### 4. Discussion

The wavelet results reveal that, the QPO signals may not appear continuously as previously thought, but appears and disappears on the order of seconds. The hardness ratio, mean count

rate and PDS all show different behaviors between QPO and non-QPO time, with higher mean count rate and higher hardness ratio for the QPO time. A similar phenomenon is called the flip-flop, which also shows distinct differences in PDS and flux. However, the transition times of flip-flops are normally range from a few tens of seconds to more than a thousand seconds, which is much longer than observed in the wavelet results. It is possible that PDS cannot achieve second-level accuracy, but further research is required. In addition, type-B QPOs always appear in the flip-flops, either in the bright state or the dim state, except for Swift J1658.2-4242 (Bogensberger et al., 2020). However, the type-B QPO is not noticed during the HIMS fast transition of this study (see Figure 3), either because the time segment of several seconds is not long enough for generating a reliable PDS, or the fast transition observed in MAXI J1535-571 exhibit the same behavior with Swift J1658.2-4242.

The S-factor, as defined in Chen et al. (2022a), is the ratio of the effective oscillation time and the total time in a selected GTI, where the effective oscillation time is defined as the following. Firstly, we define an "effective range" within the local wavelet spectrum, which represents the centroid frequency error range. Within this range, we exclude portions affected by the coi to ensure that we only consider areas with reliable signals. Then, for each time point, we examine its corresponding "effective range". If any power within the "effective range" at that time point exceeds the 95% confidence level, it is labeled as an "effective oscillation time". The calculation of the error of S-factor is based on the NICER time resolution, which is quite small compared to S-factor, thus are ignored in our figures. In Figure 4, we show the S-factor evolution with and without QPO component extracted in wavelet. The values drops overall by about 0.1 after the method applied. The shape of the evolution on the other hand, does not change too much except the type-B QPO time range as marked by Stevens et al. (2018) and Zhang et al. (2023), which are almost always zero. The zero S-factor here means no significant power detected within the QPO frequency range, indicating that the signal of type-B QPO is very week or completely hidden beneath the BBN.

To further verify the differences in the S-factor between type-B and type-C QPOs, we refer to a method provided by Stevens et al. (2018) to quantitatively separate them based on the range of hardness ratio and rms, where hardness ratio is defined as the ratio of 7-10 keV to 1-2 keV count rate, and rms in 3-10 keV is calculated in the frequency range of 1.5-15 Hz. They found that the type-B QPOs are in the range of 0.021-0.031 for hardness ratio, and less than 5 % for rms in 3-10 keV. Based on these criterion, we re-generate the light curves to calculate the hardness ratio and rms in each GTI. The hardness ratio and rms results are shown in Figure 5. We then separate the QPO types and plot the evolution of S-factor on the top panel of Figure 6. All the type-B marked QPOs has the S-factor of zero except one GTI in 1050360119, which still shows a very small value of 0.0022. Among all the type-C marked QPOs, there are 7 points with S-factors smaller than this value, including one GTI in 1050360114, one GTI in 1050360115, four GTIs in 1050360119, and one more GTI in 1130360110, which are shown in Figure 5 with green squares. Others are all greater or

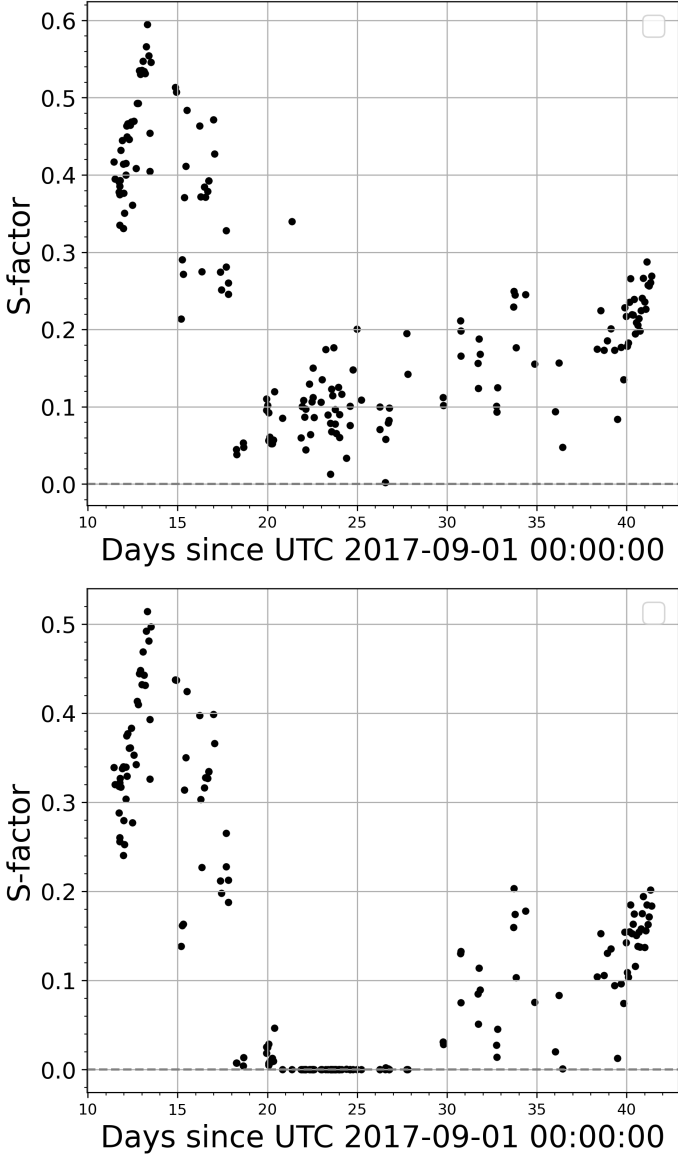


Figure 4: S-factor evolution calculated with 95% confidence level. **Top panel:** without QPO component extraction in wavelet. **Bottom panel:** after QPO component extraction in wavelet. GTI > 100s.

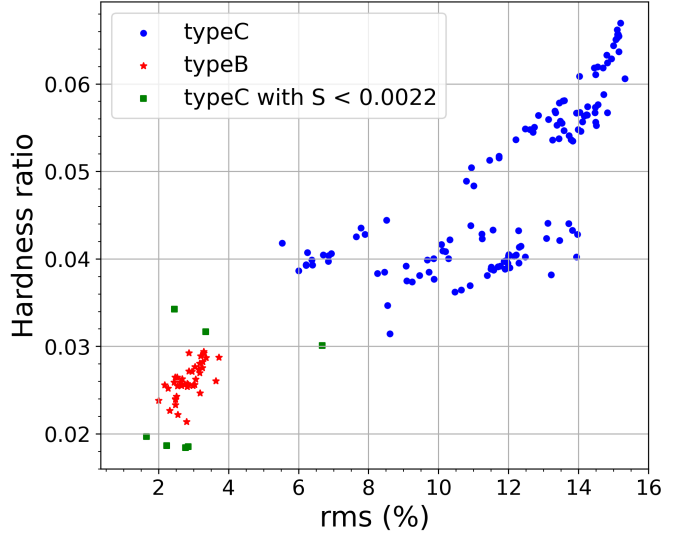


Figure 5: Hardness ratio (7-10 keV / 1-2 keV) and rms (3-10 keV in 1.5-15 Hz) relation. Blue points are type-C QPOs, green squares are type-C QPOs with S-factors less than 0.0022, and red stars are type-B QPOs.

equal to 0.01. The former six points are all located very close to the type-B QPO region as reported in Figure 2 of Stevens et al. (2018), showing rms < 5% and hardness ratio around 0.019 or 0.032. Considering Stevens et al. (2018) selected the hardness ratio region by sliding the window by 30% increments, these six points may still be in the type-B QPO region. The last point in 1130360110 however, has rms of 0.067 and hardness ratio of 0.030. It is possible that rms selection performed by Stevens et al. (2018) was not quite rigorous, because the limit was chosen based on a gap between 4% and 5.5%. The 95% confidence level result may ignore some QPO signals, thus a 68% confidence level result is recalculated for comparison, and is shown in Figure 7. It is clear that all the S-factor of type-B QPOs are smaller than 0.1, including the seven points mentioned earlier. A distinct gap in S-factor can be noticed between them and other type-C QPOs, which normally have S-factor greater than 0.18. Considering the S-factor results of both Figure 6 and Figure 7, the S-factor calculated through wavelet analysis might offer another reference parameter for the classification of QPO types that the S-factor of type-B QPO is notably smaller than that of type-C QPO. However, a more comprehensive study with different telescopes and sources will be absolutely required.

To further understand the properties of S-factor, we plot it with the QPO frequency in Figure 8, and find that it exhibits a very similar property with rms, which makes sense because they both represent the distribution properties of power, either in wavelet or in PDS. Motta et al. (2015) investigated the relation of QPO rms and QPO centroid frequency to study the differences in high and low inclination sources. The anti-correlation of type-C QPO between rms and centroid frequency greater than 2 Hz can be noted, while the correlation of type-B QPO is not significant in their study. They are both similar to the results shown by the S-factor, and the different behavior

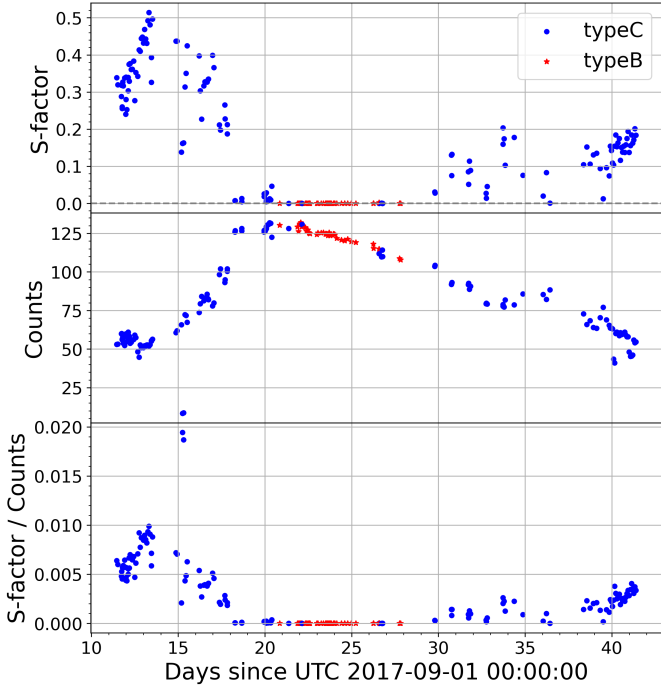


Figure 6: The evolution of S-factor calculated with 95% confidence level (top panel), counts (middle panel) and the ratio of S-factor to counts (bottom panel). Blue points are type-C QPOs, while red stars are type-B QPOs.

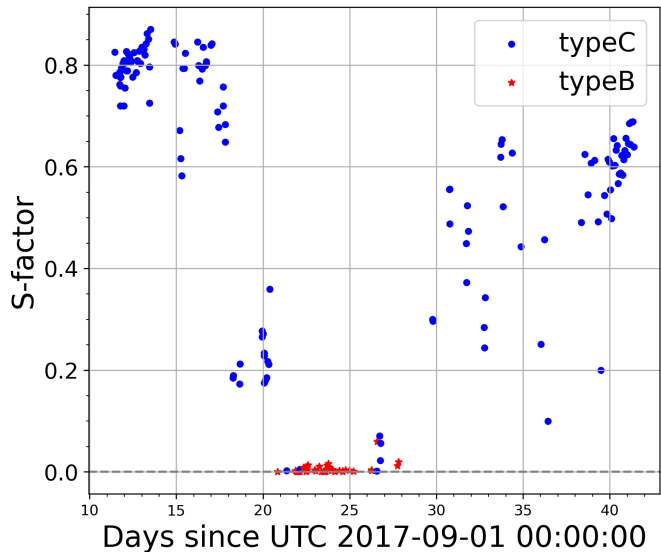


Figure 7: S-factor evolution calculated with 68% confidence level. Blue points are type-C QPOs, while red stars are type-B QPOs.

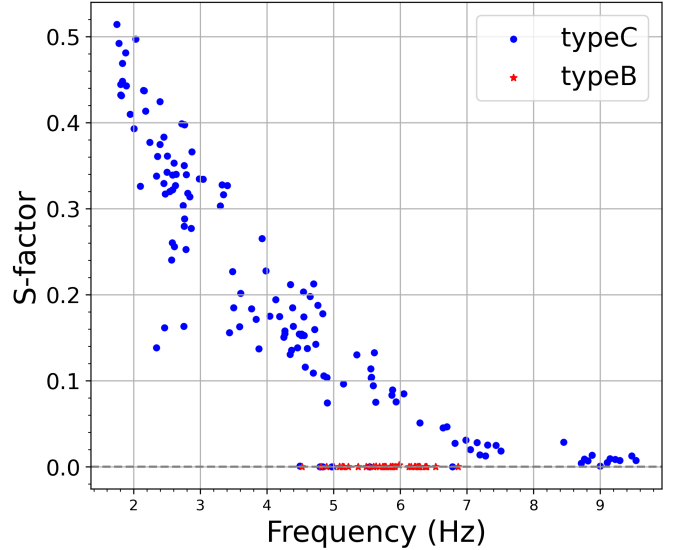


Figure 8: Frequency and S-factor (95% confidence level) relation . Each point presents one GTI. Blue points are type-C QPOs, while red stars are type-B QPOs.

of type-C and type-B QPOs may be discrete radio jet related (Stevens and Uttley, 2016; de Ruiter et al., 2019). Unfortunately, we do not have QPO centroid frequency below 1 Hz of MAXI J1535-571, otherwise we can show whether this source, as a potential high-inclination black hole binary, exhibits S-factor properties that are completely similar to QPO rms.

In addition, we notice that the relation of S-factor and count number might be energy dependent. As shown in Figure 6, when the count decrease in a small range at the very beginning, the S-factor increases significantly. Then the count increases and the S-factor decreases. When the outburst enters SIMS in which the type-B QPO dominated, the S-factor remains stable at zero. After that, the count number continue decreases and the S-factor raises again. The ratio of S-factor to counts does not remain constant for the type-C QPOs. Instead, it appears as a decrease in value in both sides when approaching the SIMS. These results show that, for type-C QPO, the S-factor and counts are inversely related, while the S-factor of type-B QPO does not change with count number. Chen et al. (2022a) find the positive correlation of S-factors of type-C QPOs and count rates based on ME and HE bands of Insight-HXMT data, and the S-factor in LE band does not change with count rate. We speculate that the latter may be due to the fact that BBN accounts for a large proportion in the calculation of S-factor, since the QPO component is quite weak in LE after P011453500902. Nevertheless, due to the weak influence of BBN on the QPO component in the ME and HE bands, the QPO appears to perform different behaviors below and above 10 keV. A possible explanation is that the generation mechanism of QPO is different at lower energy band ( $< 10$  keV) which dominated by disc component, and at higher energy band ( $> 10$  keV) dominated by corona.

Recent research shows that BH X-ray binaries may consist of two coronas, such as MAXI J1348–630 (García et al., 2021) and GX 339–4 (Peirano et al., 2023), by fitting spectra and

type-B QPOs with a dual-component comptonization model. Peirano et al. (2023) proposed that the inner hotter part of the disc provides the seed photons of the small corona, and the outer cooler part of the disc provides the seed photons of the large corona. Rawat et al. (2023) studied the same NICER observations of MAXI J1535-571 with a single-component time-dependent Comptonization model, but explained the difference between the temperature of the inner disk radius  $kT_{in}$  and the temperature of the seed photon source  $kT_s$  with a dual-corona geometry. If so, the different S-factor relation between lower band ( $< 10$  keV) and higher band ( $10 - 100$  keV) may be related to the dual-corona geometry.

## 5. Conclusions

Wavelet analysis, with the QPO component extracted only, is utilized to study the QPO evolution in MAXI J1535-571 during its 2017 outburst. Based on the confident intervals, the light curve is separated into QPO time and non-QPO time, and significant differences are noticed in the PDS, hardness ratio and mean counts, indicating the QPO signals do not continuously show in the light curve of MAXI J1535-571 but appear and disappear on the order of seconds, which support the wavelet results observed by Insight-HXMT (Chen et al., 2022b).

The wavelet method normally cannot be used to calculate the magnitude of power because of the mother wave utilized in the method, which will definitely smooth out the power. On the other hand, it can provide a more stable result with no "spiking noise" which is very common in the PDS. Hence, the parameters derived from wavelet such as the S-factor, which shows the proportion of time with significant QPO power, could be more stable. Therefore, using NICER data, we conduct a study on the S-factors of type-B and type-C QPOs in MAXI J1535-571, and find the existence of differences, which may contribute to the classification of QPOs. Additionally, we investigate the properties of the S-factor and find that it may be energy dependent and perhaps share similarities with rms. However, since wavelet analysis is rarely used in QPO research, the results regarding the S-factor require support from future research.

## Acknowledgements

We are grateful to the referee for the useful suggestions to improve the manuscript. This work is supported by the National Key Research and Development Program of China (Grants No. 2021YFA0718503), the NSFC (No. 12133007).

## References

- Bellavita, C., García, F., Méndez, M., Karpouzas, K., 2022. vKomph: a variable Comptonization model for low-frequency quasi-periodic oscillations in black hole X-ray binaries. *Monthly Notices of the Royal Astronomical Society* 515, 2099–2109. doi:10.1093/mnras/stac1922, arXiv:2206.13609.
- Belloni, T., Hasinger, G., 1990. An atlas of aperiodic variability in HMXB. *Astronomy & Astrophysics* 230, 103–119.
- Belloni, T.M., Motta, S.E., 2016. Transient Black Hole Binaries, in: *Astrophysics of Black Holes: From Fundamental Aspects to Latest Developments*.
- Belloni, T.M., Motta, S.E., Muñoz-Darias, T., 2011. Black hole transients. *Bulletin of the Astronomical Society of India* 39, 409–428. doi:10.48550/arXiv.1109.3388, arXiv:1109.3388.
- Belloni, T.M., Stella, L., 2014. Fast Variability from Black-Hole Binaries. *Space Science Reviews* 183, 43–60. doi:10.1007/s11214-014-0076-0, arXiv:1407.7373.
- Bhargava, Y., Belloni, T., Bhattacharya, D., Misra, R., 2019. Spectro-timing analysis of MAXI J1535-571 using AstroSat. *Monthly Notices of the Royal Astronomical Society* 488, 720–727. doi:10.1093/mnras/stz1774, arXiv:1906.10595.
- Boggsberger, D., Ponti, G., Jin, C., Belloni, T.M., Pan, H., Nandra, K., Russell, T.D., Miller-Jones, J.C.A., Muñoz-Darias, T., Vynatheya, P., Vincentelli, F., 2020. An underlying clock in the extreme flip-flop state transitions of the black hole transient Swift J1658.2-4242. *Astronomy & Astrophysics* 641, A101. doi:10.1051/0004-6361/202037657, arXiv:2006.10934.
- Cabanac, C., Henri, G., Petrucci, P.O., Malzac, J., Ferreira, J., Belloni, T.M., 2010. Variability of X-ray binaries from an oscillating hot corona. *Monthly Notices of the Royal Astronomical Society* 404, 738–748. doi:10.1111/j.1365-2966.2010.16340.x, arXiv:1001.2116.
- Casella, P., Belloni, T., Homan, J., Stella, L., 2004. A study of the low-frequency quasi-periodic oscillations in the X-ray light curves of the black hole candidate  $\text{J}^{+}\text{ASTROBJ}_{\text{XTE}} \text{J}^{+}1859+226/\text{ASTROBJ}_{\text{.}}$  *Astronomy & Astrophysics* 426, 587–600. doi:10.1051/0004-6361:20041231, arXiv:astro-ph/0407262.
- Casella, P., Belloni, T., Stella, L., 2005. The ABC of Low-Frequency Quasi-periodic Oscillations in Black Hole Candidates: Analogies with Z Sources. *The Astrophysical Journal* 629, 403–407. doi:10.1086/431174, arXiv:astro-ph/0504318.
- Chauhan, J., Miller-Jones, J.C.A., Anderson, G.E., Raja, W., Bahramian, A., Hotan, A., Indermuehle, B., Whiting, M., Allison, J.R., Anderson, C., Bunting, J., Koribalski, B., Mahony, E., 2019. An H I absorption distance to the black hole candidate X-ray binary MAXI J1535-571. *Monthly Notices of the Royal Astronomical Society* 488, L129–L133. doi:10.1093/mnrasl/slz113, arXiv:1905.08497.
- Chen, X., Wang, W., Tian, P.F., Zhang, P., Liu, Q., Wu, H.J., Sai, N., Huang, Y., Song, L.M., Qu, J.L., Tao, L., Zhang, S., Lu, F.J., Zhang, S.N., 2022a. Wavelet analysis of the transient QPOs in MAXI J1535-571 with Insight-HXMT. *Monthly Notices of the Royal Astronomical Society* 517, 182–191. doi:10.1093/mnras/stac2710, arXiv:2209.10408.
- Chen, X., Wang, W., You, B., Tian, P.F., Liu, Q., Zhang, P., Ding, Y.Z., Qu, J.L., Zhang, S.N., Song, L.M., Lu, F.J., Zhang, S., 2022b. Wavelet analysis of MAXI J1535-571 with Insight-HXMT. *Monthly Notices of the Royal Astronomical Society* 513, 4875–4886. doi:10.1093/mnras/stac1175, arXiv:2204.12030.
- Corral-Santana, J.M., Casares, J., Muñoz-Darias, T., Bauer, F.E., Martínez-Pais, I.G., Russell, D.M., 2016. BlackCAT: A catalogue of stellar-mass black holes in X-ray transients. *Astronomy & Astrophysics* 587, A61. doi:10.1051/0004-6361/201527130, arXiv:1510.08869.
- Cúneo, V.A., Alabarta, K., Zhang, L., Altamirano, D., Méndez, M., Armas Padilla, M., Remillard, R., Homan, J., Steiner, J.F., Combi, J.A., Muñoz-Darias, T., Gendreau, K.C., Arzoumanian, Z., Stevens, A.L., Loewenstein, M., Tombesi, F., Bult, P., Fabian, A.C., Buisson, D.J.K., Neilsen, J., Basak, A., 2020. A NICER look at the state transitions of the black hole candidate MAXI J1535-571 during its reflares. *Monthly Notices of the Royal Astronomical Society* 496, 1001–1012. doi:10.1093/mnras/staa1606, arXiv:2006.03074.
- de Ruiter, I., van den Eijnden, J., Ingram, A., Uttley, P., 2019. A systematic study of the phase difference between QPO harmonics in black hole X-ray binaries. *Monthly Notices of the Royal Astronomical Society* 485, 3834–3844. doi:10.1093/mnras/stz665, arXiv:1903.03135.
- Dincer, T., 2017. The near-infrared counterpart of X-ray transient MAXI J1535-571. *The Astronomer's Telegram* 10716, 1.
- Dong, Y., Liu, Z., Tuo, Y., Steiner, J.F., Ge, M., García, J.A., Cao, X., 2022. Analysis of the reflection spectra of MAXI J1535-571 in the hard and intermediate states. *Monthly Notices of the Royal Astronomical Society* 514, 1422–1432. doi:10.1093/mnras/stac1466, arXiv:2205.12058.
- Fender, R.P., Belloni, T.M., Gallo, E., 2004. Towards a unified model for black hole X-ray binary jets. *Monthly Notices of the Royal Astronomical Society* 355, 1105–1118. doi:10.1111/j.1365-2966.2004.08384.x, arXiv:astro-ph/0409360.
- García, F., Méndez, M., Karpouzas, K., Belloni, T., Zhang, L., Altamirano,

- D., 2021. A two-component Comptonization model for the type-B QPO in MAXI J1348-630. *Monthly Notices of the Royal Astronomical Society* 501, 3173–3182. doi:10.1093/mnras/staa3944, arXiv:2012.10354.
- Gendreau, K., Arzoumanian, Z., Markwardt, C., Okajima, T., Strohmayer, T., Remillard, R., Chakrabarty, D., Prigozhin, G., Lamarr, B., Pasham, D., Steiner, J., Homan, J., Miller, J., Bult, P., Cackett, E., Iwakiri, W., Enoto, T., Uttley, P., Nicer Team, 2017. Initial NICER observations of a broadened iron line and QPOs in MAXI J1535a571. *The Astronomer's Telegram* 10768, 1.
- Gendreau, K.C., Arzoumanian, Z., Adkins, P.W., Albert, C.L., Anders, J.F., Aylward, A.T., Baker, C.L., Balsamo, E.R., Bamford, W.A., Benegalrao, S.S., Berry, D.L., Bhalwani, S., Black, J.K., Blaurock, C., Bronke, G.M., Brown, G.L., Budinoff, J.G., Cantwell, J.D., Cazeau, T., Chen, P.T., Clement, T.G., Colangelo, A.T., Coleman, J.S., Coopersmith, J.D., Dehaven, W.E., Doty, J.P., Egan, M.D., Enoto, T., Fan, T.W., Ferro, D.M., Foster, R., Galassi, N.M., Gallo, L.D., Green, C.M., Grosh, D., Ha, K.Q., Hasouneh, M.A., Heefner, K.B., Hestnes, P., Hoge, L.J., Jacobs, T.M., Jørgensen, J.L., Kaiser, M.A., Kellogg, J.W., Kenyon, S.J., Koenecue, R.G., Kozon, R.P., LaMarr, B., Lambertson, M.D., Larson, A.M., Lentine, S., Lewis, J.H., Lilly, M.G., Liu, K.A., Malonis, A., Manthripragada, S.S., Markwardt, C.B., Matonak, B.D., McGinnis, I.E., Miller, R.L., Mitchell, A.L., Mitchell, J.W., Mohammed, J.S., Monroe, C.A., Montt de Garcia, K.M., Mulé, P.D., Nagao, L.T., Ngo, S.N., Norris, E.D., Norwood, D.A., Novotka, J., Okajima, T., Olsen, L.G., Onyeachu, C.O., Orosco, H.Y., Peterson, J.R., Pevear, K.N., Pham, K.K., Pollard, S.E., Pope, J.S., Powers, D.F., Powers, C.E., Price, S.R., Prigozhin, G.Y., Ramirez, J.B., Reid, W.J., Remillard, R.A., Rogstad, E.M., Rosecrans, G.P., Rowe, J.N., Sager, J.A., Sanders, C.A., Savadkin, B., Saylor, M.R., Schaeffer, A.F., Schweiss, N.S., Semper, S.R., Serlemitsos, P.J., Shackelford, L.V., Soong, Y., Strubel, J., Vezie, M.L., Villasenor, J.S., Winternitz, L.B., Wofford, G.I., Wright, M.R., Yang, M.Y., Yu, W.H., 2016. The Neutron star Interior Composition Explorer (NICER): design and development, in: *Space Telescopes and Instrumentation 2016: Ultraviolet to Gamma Ray*.
- Homan, J., Belloni, T., 2005. The Evolution of Black Hole States. *Astrophysics and Space Science* 300, 107–117. doi:10.1007/s10509-005-1197-4, arXiv:astro-ph/0412597.
- Homan, J., Miller, J.M., Wijnands, R., van der Klis, M., Belloni, T., Steeghs, D., Lewin, W.H.G., 2005. High- and Low-Frequency Quasi-periodic Oscillations in the X-Ray Light Curves of the Black Hole Transient H1743-322. *The Astrophysical Journal* 623, 383–391. doi:10.1086/424994, arXiv:astro-ph/0406334.
- Homan, J., Wijnands, R., van der Klis, M., Belloni, T., van Paradijs, J., Klein-Wolt, M., Fender, R., Méndez, M., 2001. Correlated X-Ray Spectral and Timing Behavior of the Black Hole Candidate XTE J1550-564: A New Interpretation of Black Hole States. *The Astrophysical Journal Supplement* 132, 377–402. doi:10.1086/318954, arXiv:astro-ph/0001163.
- Huang, Y., Qu, J.L., Zhang, S.N., Bu, Q.C., Chen, Y.P., Tao, L., Zhang, S., Lu, F.J., Li, T.P., Song, L.M., Xu, Y.P., Cao, X.L., Chen, Y., Liu, C.Z., Chang, H.K., Yu, W.F., Weng, S.S., Hou, X., Kong, A.K.H., Xie, F.G., Zhang, G.B., ZHOU, J.F., Chang, Z., Chen, G., Chen, L., Chen, T.X., Chen, Y.B., Cui, W., Cui, W.W., Deng, J.K., Dong, Y.W., Du, Y.Y., Fu, M.X., Gao, G.H., Gao, H., Gao, M., Ge, M.Y., Gu, Y.D., Guan, J., Gungor, C., Guo, C.C., Han, D.W., Hu, W., Huo, J., Ji, J.F., Jia, S.M., Jiang, L.H., Jiang, W.C., Jin, J., Jin, Y.J., Li, B., Li, C.K., Li, G., Li, M.S., Li, W., Li, X., Li, X.B., Li, X.F., Li, Y.G., Li, Z.J., Li, Z.W., Liang, X.H., Liao, J.Y., Liu, G.Q., Liu, H.W., Liu, S.Z., Liu, X.J., Liu, Y., Liu, Y.N., Lu, B., Lu, X.F., Luo, T., Ma, X., Meng, B., Nang, Y., Nie, J.Y., Ou, G., Sai, N., Shang, R.C., Sun, L., Tan, Y., Tao, W., Tuo, Y.L., Wang, G.F., Wang, H.Y., Wang, J., Wang, W.S., Wang, Y.S., Wen, X.Y., Wu, B.B., Wu, M., Xiao, G.C., Xiong, S.L., Xu, H., Yan, L.L., Yang, J.W., Yang, S., Yang, Y.J., Zhang, A.M., Zhang, C.L., Zhang, C.M., Zhang, F., Zhang, H.M., Zhang, J., Zhang, Q., Zhang, T., Zhang, W., Zhang, W.C., Zhang, W.Z., Zhang, Y., Zhang, Y., Zhang, Y.F., Zhang, Y.J., Zhang, Z., Zhang, Z., Zhang, Z.L., Zhao, H.S., Zhao, J.L., Zhao, X.F., Zheng, S.J., Zhu, Y., Zhu, Y.X., Zou, C.L., Insight-HXMT Collaboration, 2018. INSIGHT-HXMT Observations of the New Black Hole Candidate MAXI J1535-571: Timing Analysis. *The Astrophysical Journal* 866, 122. doi:10.3847/1538-4357/aade4c, arXiv:1808.05318.
- Ingram, A., Done, C., Fragile, P.C., 2009. Low-frequency quasi-periodic oscillations spectra and Lense-Thirring precession. *Monthly Notices of the Royal Astronomical Society* 397, L101–L105. doi:10.1111/j.1745-3933.2009.00693.x, arXiv:0901.1238.
- Ingram, A., van der Klis, M., Middleton, M., Altamirano, D., Uttley, P., 2017. Tomographic reflection modelling of quasi-periodic oscillations in the black hole binary H 1743-322. *Monthly Notices of the Royal Astronomical Society* 464, 2979–2991. doi:10.1093/mnras/stw2581, arXiv:1610.00948.
- Ingram, A., van der Klis, M., Middleton, M., Done, C., Altamirano, D., Heil, L., Uttley, P., Axelsson, M., 2016. A quasi-periodic modulation of the iron line centroid energy in the black hole binary H1743-322. *Monthly Notices of the Royal Astronomical Society* 461, 1967–1980. doi:10.1093/mnras/stw1245, arXiv:1607.02866.
- Ingram, A.R., Motta, S.E., 2019. A review of quasi-periodic oscillations from black hole X-ray binaries: Observation and theory. *New Astronomy Reviews* 85, 101524. doi:10.1016/j.newar.2020.101524, arXiv:2001.08758.
- Kalamkar, M., Homan, J., Altamirano, D., van der Klis, M., Casella, P., Linares, M., 2011. The Identification of MAXI J1659-152 as a Black Hole Candidate. *The Astrophysical Journal Letters* 731, L2. doi:10.1088/2041-8205/731/1/L2, arXiv:1012.4330.
- Karpouzas, K., Méndez, M., Ribeiro, E.M., Altamirano, D., Blaes, O., García, F., 2020. The Comptonizing medium of the neutron star in 4U 1636 - 53 through its lower kilohertz quasi-periodic oscillations. *Monthly Notices of the Royal Astronomical Society* 492, 1399–1415. doi:10.1093/mnras/stz3502, arXiv:1912.05380.
- Katoch, T., Baby, B.E., Nandi, A., Agrawal, V.K., Antia, H.M., Mukerjee, K., 2021. AstroSat view of IGR J17091-3624 and GRS 1915 + 105: decoding the ‘pulse’ in the ‘Heartbeat State’. *Monthly Notices of the Royal Astronomical Society* 501, 6123–6138. doi:10.1093/mnras/staa3756, arXiv:2011.13282.
- Kennea, J.A., Evans, P.A., Beardmore, A.P., Krimm, H.A., Romano, P., Yamamoto, K., Serino, M., Negoro, H., 2017. MAXI J1535-571: Swift detection and localization. *The Astronomer's Telegram* 10700, 1.
- Lachowicz, P., Done, C., 2010. Quasi-periodic oscillations under wavelet microscope: the application of Matching Pursuit algorithm. *Astronomy & Astrophysics* 515, A65. doi:10.1051/0004-6361/200913144, arXiv:0908.2740.
- Méndez, M., Karpouzas, K., García, F., Zhang, L., Zhang, Y., Belloni, T.M., Altamirano, D., 2022. Coupling between the accreting corona and the relativistic jet in the microquasar GRS 1915+105. *Nature Astronomy* 6, 577–583. doi:10.1038/s41550-022-01617-y, arXiv:2203.02963.
- Mereminskii, I.A., Grebenev, S.A., Prosvetov, A.V., Semena, A.N., 2018. Low-Frequency Quasi-Periodic Oscillations in the X-ray Nova MAXI J1535-571 at the Initial Stage of Its 2017 Outburst. *Astronomy Letters* 44, 378–389. doi:10.1134/S106377371806004X, arXiv:1806.06025.
- Miller, J.M., Gendreau, K., Ludlam, R.M., Fabian, A.C., Altamirano, D., Arzoumanian, Z., Bult, P.M., Cackett, E.M., Homan, J., Kara, E., Neilsen, J., Remillard, R.A., Tombesi, F., 2018. A NICER Spectrum of MAXI J1535-571: Near-maximal Black Hole Spin and Potential Disk Warping. *The Astrophysical Journal Letters* 860, L28. doi:10.3847/2041-8213/aacc61, arXiv:1806.04115.
- Miyamoto, S., Kimura, K., Kitamoto, S., Dotani, T., Ebisawa, K., 1991. X-Ray Variability of GX 339-4 in Its Very High State. *The Astrophysical Journal* 383, 784. doi:10.1086/170837.
- Motta, S., Homan, J., Muñoz-Darias, T., Casella, P., Belloni, T.M., Hiemstra, B., Méndez, M., 2012. Discovery of two simultaneous non-harmonically related quasi-periodic oscillations in the 2005 outburst of the black hole binary GRO J1655-40. *Monthly Notices of the Royal Astronomical Society* 427, 595–606. doi:10.1111/j.1365-2966.2012.22037.x, arXiv:1209.0327.
- Motta, S., Muñoz-Darias, T., Casella, P., Belloni, T., Homan, J., 2011. Low-frequency oscillations in black holes: a spectral-timing approach to the case of GX 339-4. *Monthly Notices of the Royal Astronomical Society* 418, 2292–2307. doi:10.1111/j.1365-2966.2011.19566.x, arXiv:1108.0540.
- Motta, S.E., 2016. Quasi periodic oscillations in black hole binaries. *Astronomische Nachrichten* 337, 398. doi:10.1002/asna.201612320, arXiv:1603.07885.
- Motta, S.E., Casella, P., Henze, M., Muñoz-Darias, T., Sanna, A., Fender, R., Belloni, T., 2015. Geometrical constraints on the origin of timing signals from black holes. *Monthly Notices of the Royal Astronomical Society* 447, 2059–2072. doi:10.1093/mnras/stu2579, arXiv:1404.7293.
- Negoro, H., Ishikawa, M., Ueno, S., Tomida, H., Sugawara, Y., Isobe, N., Shi-

- momukai, R., Mihara, T., Sugizaki, M., Serino, M., Iwakiri, S.N.W., Shidatsu, M., Matsuoka, M., Kawai, N., Sugita, S., Yoshii, T., Tachibana, Y., Harita, S., Muraki, Y., Morita, K., Yoshida, A., Sakamoto, T., Kawakubo, Y., Kitaoka, Y., Hashimoto, T., Tsunemi, H., Yoneyama, T., Nakajima, M., Kawase, T., Sakamaki, A., Ueda, Y., Hori, T., Tanimoto, A., Oda, S., Tsuboi, Y., Nakamura, Y., Sasaki, R., Kawai, H., Yamauchi, M., Hanyu, C., Hidaka, K., Kawamuro, T., Yamaoka, K., 2017a. MAXI/GSC discovery of a new hard X-ray transient MAXI J1535-571. *The Astronomer's Telegram* 10699, 1.
- Negoro, H., Kawase, T., Sugizaki, M., Ueno, S., Tomida, H., Sugawara, Y., Isobe, N., Ishikawa, M., Shimomukai, R., Mihara, T., Serino, M., Iwakiri, S.N.W., Shidatsu, M., Matsuoka, M., Kawai, N., Sugita, S., Yoshii, T., Tachibana, Y., Harita, S., Muraki, Y., Morita, K., Yoshida, A., Sakamoto, T., Kawakubo, Y., Kitaoka, Y., Hashimoto, T., Tsunemi, H., Yoneyama, T., Nakajima, M., Sakamaki, A., Ueda, Y., Hori, T., Tanimoto, A., Oda, S., Tsuboi, Y., Nakamura, Y., Sasaki, R., Kawai, H., Yamauchi, M., Hanyu, C., Hidaka, K., Kawamuro, T., Yamaoka, K., 2017b. Further brightening of the X-ray transient MAXI J1535-571, suggesting the presence of a black hole. *The Astronomer's Telegram* 10708, 1.
- Nespoli, E., Belloni, T., Homan, J., Miller, J.M., Lewin, W.H.G., Méndez, M., van der Klis, M., 2003. A transient variable 6 Hz QPO from GX 339-4. *Astronomy & Astrophysics* 412, 235–240. doi:10.1051/0004-6361:20031423, arXiv:astro-ph/0309437.
- Nowak, M.A., 2000. Are there three peaks in the power spectra of GX 339-4 and Cyg X-1? *Monthly Notices of the Royal Astronomical Society* 318, 361–367. doi:10.1046/j.1365-8711.2000.03668.x, arXiv:astro-ph/0005232.
- Parikh, A.S., Russell, T.D., Wijnands, R., Miller-Jones, J.C.A., Sivakoff, G.R., Tetarenko, A.J., 2019. Rapidly Evolving Disk-Jet Coupling during Re-brightenings in the Black Hole Transient MAXI J1535-571. *The Astrophysical Journal Letters* 878, L28. doi:10.3847/2041-8213/ab2636, arXiv:1906.01000.
- Peirano, V., Méndez, M., García, F., Belloni, T., 2023. Dual-corona Comptonization model for the type-b quasi-periodic oscillations in GX 339-4. *Monthly Notices of the Royal Astronomical Society* 519, 1336–1348. doi:10.1093/mnras/stac3553, arXiv:2212.00062.
- Rawat, D., Méndez, M., García, F., Altamirano, D., Karpouzas, K., Zhang, L., Alabarta, K., Belloni, T.M., Jain, P., Bellavita, C., 2023. The comptonizing medium of the black hole X-ray binary MAXI J1535-571 through type-C quasi-periodic oscillations. *Monthly Notices of the Royal Astronomical Society* 520, 113–128. doi:10.1093/mnras/stad126, arXiv:2301.04418.
- Remillard, R.A., McClintock, J.E., 2006. X-Ray Properties of Black-Hole Binaries. *Annual Review of Astronomy & Astrophysics* 44, 49–92. doi:10.1146/annurev.astro.44.051905.092532, arXiv:astro-ph/0606352.
- Remillard, R.A., Sobczak, G.J., Munro, M.P., McClintock, J.E., 2002. Characterizing the Quasi-periodic Oscillation Behavior of the X-Ray Nova XTE J1550-564. *The Astrophysical Journal* 564, 962–973. doi:10.1086/324276, arXiv:astro-ph/0105508.
- Russell, T.D., Miller-Jones, J.C.A., Sivakoff, G.R., Tetarenko, A.J., Jacpot Xrb Collaboration, 2017. ATCA radio detection of MAXI J1535-571 indicates it is a strong black hole X-ray binary candidate. *The Astronomer's Telegram* 10711, 1.
- Russell, T.D., Tetarenko, A.J., Miller-Jones, J.C.A., Sivakoff, G.R., Parikh, A.S., Rapisarda, S., Wijnands, R., Corbel, S., Tremou, E., Altamirano, D., Baglio, M.C., Ceccobello, C., Degenaar, N., van den Eijnden, J., Fender, R., Heywood, I., Krimm, H.A., Lucchini, M., Markoff, S., Russell, D.M., Soria, R., Woudt, P.A., 2019. Disk-Jet Coupling in the 2017/2018 Outburst of the Galactic Black Hole Candidate X-Ray Binary MAXI J1535-571. *The Astrophysical Journal* 883, 198. doi:10.3847/1538-4357/ab3d36, arXiv:1906.00998.
- Scaringi, S., ASTR211 Students, 2017. Discovery of the optical counterpart of MAXI J1535-571. *The Astronomer's Telegram* 10702, 1.
- Sriram, K., Rao, A.R., Choi, C.S., 2012. Fast transition of type-B quasi-periodic oscillation in the black hole transient XTE J1817-330. *Astronomy & Astrophysics* 541, A6. doi:10.1051/0004-6361/201218799.
- Sriram, K., Rao, A.R., Choi, C.S., 2013. A Spectral Study of the Rapid Transitions of Type-B Quasi-periodic Oscillations in the Black Hole Transient XTE J1859+226. *The Astrophysical Journal* 775, 28. doi:10.1088/0004-637X/775/1/28, arXiv:1203.1674.
- Sriram, K., Rao, A.R., Choi, C.S., 2016. Study of a Sudden QPO Transition Event in the Black Hole Source XTE J1550-564. *The Astrophysical Journal* 823, 67. doi:10.3847/0004-637X/823/1/67.
- Stevens, A.L., Uttley, P., 2016. Phase-resolved spectroscopy of Type B quasi-periodic oscillations in GX 339-4. *Monthly Notices of the Royal Astronomical Society* 460, 2796–2810. doi:10.1093/mnras/stw1093, arXiv:1605.01753.
- Stevens, A.L., Uttley, P., Altamirano, D., Arzoumanian, Z., Bult, P., Cackett, E.M., Fabian, A.C., Gendreau, K.C., Ha, K.Q., Homan, J., Ingram, A.R., Kara, E., Kellogg, J., Ludlam, R.M., Miller, J.M., Neilsen, J., Pasham, D.R., Remillard, R.A., Steiner, J.F., van den Eijnden, J., 2018. A NICER Discovery of a Low-frequency Quasi-periodic Oscillation in the Soft-intermediate State of MAXI J1535-571. *The Astrophysical Journal Letters* 865, L15. doi:10.3847/2041-8213/aae1a4, arXiv:1809.07556.
- Stiele, H., Kong, A.K.H., 2018. A Spectral and Timing Study of MAXI J1535-571, Based on Swift/XRT, XMM-Newton, and NICER Observations Obtained in Fall 2017. *The Astrophysical Journal* 868, 71. doi:10.3847/1538-4357/aae7d3, arXiv:1810.07203.
- Tagger, M., Pellat, R., 1999. An accretion-ejection instability in magnetized disks. *Astronomy & Astrophysics* 349, 1003–1016. doi:10.48550/arXiv.astro-ph/9907267, arXiv:astro-ph/9907267.
- Takizawa, M., Dotani, T., Mitsuda, K., Matsuba, E., Ogawa, M., Aoki, T., Asai, K., Ebisawa, K., Makishima, K., Miyamoto, S., Iga, S., Vaughan, B., Rutledge, R.E., Lewin, W.H.G., 1997. Spectral and Temporal Variability in the X-Ray Flux of GS 1124-683, Nova Muscae 1991. *The Astrophysical Journal* 489, 272–283. doi:10.1086/304759.
- Torrence, C., Compo, G.P., 1998. A Practical Guide to Wavelet Analysis. *Bulletin of the American Meteorological Society* 79, 61–78. doi:10.1175/1520-0477(1998)079<0061:APGTWA>2.0.CO;2.
- van der Klis, M., 1989. Fourier techniques in X-ray timing, in: *Timing Neutron Stars*.
- Veledina, A., Poutanen, J., Ingram, A., 2013. A Unified Lense-Thirring Precession Model for Optical and X-Ray Quasi-periodic Oscillations in Black Hole Binaries. *The Astrophysical Journal* 778, 165. doi:10.1088/0004-637X/778/2/165, arXiv:1310.3821.
- Wijnands, R., Homan, J., van der Klis, M., 1999. The Complex Phase-Lag Behavior of the 3-12 Hz Quasi-Periodic Oscillations during the Very High State of XTE J1550-564. *The Astrophysical Journal Letters* 526, L33–L36. doi:10.1086/312365, arXiv:astro-ph/9909515.
- Xu, Y., Harrison, F.A., García, J.A., Fabian, A.C., Fürst, F., Gandhi, P., Grefenstette, B.W., Madsen, K.K., Miller, J.M., Parker, M.L., Tomsick, J.A., Walton, D.J., 2018. Reflection Spectra of the Black Hole Binary Candidate MAXI J1535-571 in the Hard State Observed by NuSTAR. *The Astrophysical Journal Letters* 852, L34. doi:10.3847/2041-8213/aaa4b2, arXiv:1711.01346.
- Yang, Z.X., Zhang, L., Bu, Q.C., Huang, Y., Liu, H.X., Yu, W., Wang, P.J., Tao, L., Qu, J.L., Zhang, S., Zhang, S.N., Ma, X., Song, L.M., Jia, S.M., Ge, M.Y., Liu, Q.Z., Yan, J.Z., Zhou, D.K., Li, T.M., Wu, B.Y., Ren, X.Q., Ma, R.C., Zhang, Y.X., Xu, Y.C., Ma, B.Y., Du, Y.F., Fu, Y.C., Xiao, Y.X., 2022. The Accretion Flow Geometry of MAXI J1820+070 through Broadband Noise Research with Insight Hard X-ray Modulation Telescope. *The Astrophysical Journal* 932, 7. doi:10.3847/1538-4357/ac63af, arXiv:2204.00739.
- Zhang, Y., Méndez, M., García, F., Altamirano, D., Belloni, T.M., Alabarta, K., Zhang, L., Bellavita, C., Rawat, D., Ma, R., 2023. A NICER look at the jet-like corona of MAXI J1535-571 through type-B quasi-periodic oscillations. *Monthly Notices of the Royal Astronomical Society* 520, 5144–5156. doi:10.1093/mnras/stad460, arXiv:2302.04007.
- Zhang, Y., Méndez, M., García, F., Zhang, S.N., Karpouzas, K., Altamirano, D., Belloni, T.M., Qu, J., Zhang, S., Tao, L., Zhang, L., Huang, Y., Kong, L., Ma, R., Yu, W., Rawat, D., Bellavita, C., 2022. The evolution of the corona in MAXI J1535-571 through type-C quasi-periodic oscillations with Insight-HXMT. *Monthly Notices of the Royal Astronomical Society* 512, 2686–2696. doi:10.1093/mnras/stac690, arXiv:2203.05308.